Analyzing vibration modes in non-homogeneous parallelogram plates

Sapna[1], Amit Sharma[2]
Amity University Haryana, Gurugram, India
[2]Corresponding author
E-mail: [1]*sapnasisotiya99@gmail.com*, [2]*dba.amitsharma@gmail.com*

Received 31 October 2023; accepted 11 November 2023; published online 27 November 2023
DOI https://doi.org/10.21595/vp.2023.23758

Check for updates

67th International Conference on Vibroengineering in Udaipur, India, November 27, 2023

Abstract. This study analyzes vibration modes in non-homogeneous orthotropic parallelogram plate with a one-dimensional circular thickness, focusing on SCCC edge condition, where C and S represent the clamped and simply supported edges of the plate, respectively. Circular Poisson's ratio variation is considered, along with linear temperature changes. The study demonstrates the advantages of variable Poisson's ratio over density parameter variation in obtaining shorter vibration time periods. Orthotropic parallelogram plate, thermal gradient, circular tapering, nonhomogeneity.

Keywords: orthotropic parallelogram plate, thermal gradient, circular tapering, nonhomogeneity.

1. Introduction

The analysis of vibrational modes in various plate configurations, including tapered ones, is vital in engineering, given their wide-ranging applications. Numerous studies have contributed to this area.

Di et al. [2] introduced a theory enhancing the accuracy of predicting the behavior of thick orthotropic plates compared to classical lamination and shear deformation theories. Gupta et al. [3] investigated transverse motion in an elastic plate with non-linear thickness and thermal gradient, utilizing the Rayleigh-Ritz technique. Gupta et al. [4] introduced a model for analyzing vibrations in parallelogram-shaped, viscoelastic, orthotropic plates with linear thickness variations in both directions. Khanna [6] used the Rayleigh Ritz method to study frequency modes of a viscoelastic isotropic rectangular plate, considering the impact of thermal gradient. The natural vibration of non-homogeneous tapered parallelogram plates with temperature variation was examined in [8]. Vibrational frequencies in a non-uniformly thick parallelogram plate were mathematically analyzed, considering linear temperature effects by authors in [9]. The influence of thermal effects on non-homogeneous parallelogram plates with two-dimensional circular variations in thickness was explored in a study referenced as [10]. In [11], the authors focused on the vibration of orthotropic square plates with varying thickness, using the Rayleigh-Ritz method and MATLAB software. Sharma et al. [12] examined an orthotropic parallelogram plate with bi-linear thickness variation and a parabolic temperature distribution, specifically focusing on the $SSSS$ edge condition.

This paper investigates the impact of one-dimensional circular tapering, Poisson's ratio, and linear temperature on vibrational modes in a non-homogeneous orthotropic parallelogram plate under $SCCC$ boundary conditions.

2. Geometry and analytical approach

Consider a nonhomogeneous parallelogram plate depicted in Fig. 1 with dimensions a and b, thickness l, and density ρ.

The skew plate, represented in Fig. 1, has a circular thickness denoted as l in one dimension. Additionally, Poisson's ratio ν is assumed to be circular in one dimension:

$$l = l_0 \left[1 + \beta \left(1 - \sqrt{1 - \frac{\xi^2}{a^2}} \right) \right], \quad \nu_\xi = \nu_{\xi_0} \left[1 - m \left(1 - \sqrt{1 - \frac{\xi^2}{a^2}} \right) \right], \tag{1}$$

where, l_0 and ν_{ξ_0} stand for the initial thickness and Poisson's ratio of the plate at the origin. Furthermore, β (ranging from 0 to 1) and m (ranging from 0 to 1) represent the taper and non-homogeneity parameters, respectively. We assume a two-dimensional steady-state temperature distribution on the plate, following the parabolic model introduced in [7]:

$$\tau = \tau_0 \left(1 - \frac{\xi}{a} \right) \left(1 - \frac{\psi}{b} \right), \tag{2}$$

where, τ and τ_0 denote the temperature excess above the reference temperature at any point on the plate and at the origin, respectively. The temperature dependence modulus of elasticity for engineering structures follows [7]:

$$E_\xi(\tau) = E_1(1 - \gamma\tau), \quad E_\psi(\tau) = E_2(1 - \gamma\tau), \quad G_{\xi\psi}(\tau) = G_0(1 - \gamma\tau), \tag{3}$$

where, E_ξ and E_ψ denote Young's moduli in the ξ and ψ directions, while G_{ξ_ψ} represents the shear modulus. The parameter γ accounts for the slope variation of moduli with temperature. By substituting Eq. (2) in Eq. (3), we obtain the following expressions:

$$\begin{gathered} E_\xi(\tau) = E_1 \left[1 - \alpha \left(1 - \frac{\xi}{a} \right) \left(1 - \frac{\psi}{b} \right) \right], \quad E_\psi(\tau) = E_2 \left[1 - \alpha \left(1 - \frac{\xi}{a} \right) \left(1 - \frac{\psi}{b} \right) \right], \\ G_{\xi\psi}(\tau) = G_0 \left[1 - \alpha \left(1 - \frac{\xi}{a} \right) \left(1 - \frac{\psi}{b} \right) \right], \end{gathered} \tag{4}$$

where $\alpha = \gamma\tau_0$, $(0 \le \alpha < 1)$ is called temperature gradient.

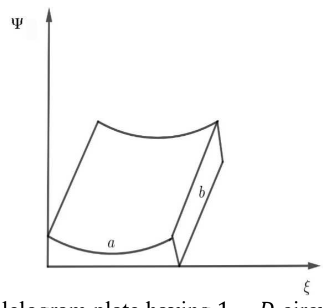

Fig. 1. Parallelogram plate having $1 - D$ circular thickness

The flexural rigidities D_ξ, D_ψ and torsional rigidity $D_{\xi\psi}$ of the plate are taken as in [12]:

$$D_\xi = \frac{E_\xi l^3}{12(1 - \nu_\xi \nu_\psi)}, \quad D_\psi = \frac{E_\eta l^3}{12(1 - \nu_\xi \nu_\psi)}, \quad D_{\xi\psi} = \frac{G_{\xi\psi} l^3}{12}, \quad D_1 = \nu_\xi D_\psi = \nu_\psi D_\xi, \tag{5}$$

where ν_ξ and ν_η are Poisson's ratios. Using Eqs. (1), (3) and (4) in Eq. (5), we get:

$$D_\xi = \frac{E_1 h_0^3}{12(1 - \nu_{\xi_0}(1 - m\Upsilon_1)\nu_\psi)} \left[\left\{ 1 - \alpha \left(1 - \frac{\xi}{a} \right) \left(1 - \frac{\psi}{b} \right) \right\} \left\{ 1 + \beta \left(1 - \sqrt{1 - \frac{\xi^2}{a^2}} \right) \right\}^3 \right], \tag{6}$$

$$D_\psi = \frac{E_2 h_0^3}{12\left(1-\nu_{\xi_0}(1-m\Upsilon_1)\nu_\psi\right)}\left[\left\{1-\alpha\left(1-\frac{\xi}{a}\right)\left(1-\frac{\psi}{b}\right)\right\}\left\{1+\beta\left(1-\sqrt{1-\frac{\xi}{a}}\right)\right\}^3\right], \quad (7)$$

$$D_{\xi\psi} = \frac{G_0 h_0^3}{12}\left[\left\{1-\alpha\left(1-\frac{\xi}{a}\right)\left(1-\frac{\psi}{b}\right)\right\}\left\{1+\beta\left(1-\sqrt{1-\frac{\xi^2}{a^2}}\right)\right\}^3\right], \quad (8)$$

$$D_1 = \frac{E_1 h_0^3 \nu_\psi}{12\left(1-\nu_{\xi_0}(1-m\Upsilon_1)\nu_\psi\right)}\left[\left\{1-\alpha\left(1-\frac{\xi}{a}\right)\left(1-\frac{\psi}{b}\right)\right\}\left\{1+\beta\left(1-\sqrt{1-\frac{\xi^2}{a^2}}\right)\right\}^3\right], \quad (9)$$

Now, introducing non-dimensional variable as:

$$E_1^* = \frac{E_1}{1-\nu_{\xi_0}(1-m\Upsilon_1)\nu_\psi}, \quad E_2^* = \frac{E_2}{1-\nu_{\xi_0}(1-m\Upsilon_1)\nu_\psi}, \quad E^* = \nu_{\xi_0}(1-m\Upsilon_1)E_2^* = \nu_\psi E_1^*. \quad (10)$$

The equation for kinetic energy T_s and strain energy V_s for natural transverse vibration of non-uniform orthotropic parallelogram is taken as in [1]:

$$T_s = \frac{1}{2}\omega^2 \int_0^a \int_0^b \rho l \, \Phi^2 \cos\theta d\xi d\psi, \quad (11)$$

$$\begin{aligned} V_s = \frac{1}{2}\int_0^a \int_0^b \Bigg[& D_\xi \left(\frac{\partial^2\Phi}{\partial\xi^2}\right)^2 + D_\psi \left(\frac{\partial^2\Phi}{\partial\xi^2}\tan^2\theta - 2\frac{\partial^2\Phi}{\partial\xi\partial\psi}\tan\theta\sec\theta + \frac{\partial^2\Phi}{\partial\psi^2}\sec^2\theta\right)^2 \\ & +2D_1\left(\frac{\partial^2\Phi}{\partial\xi^2}\right)\left(\frac{\partial^2\Phi}{\partial\xi^2}\tan^2\theta + 2\frac{\partial^2\Phi}{\partial\xi\partial\psi}\tan\theta\sec\theta + \frac{\partial^2\Phi}{\partial\psi^2}\sec^2\theta\right) \\ & +4D_{\xi\psi}\left(-\frac{\partial^2\Phi}{\partial\xi^2}\tan\theta + \frac{\partial^2\Phi}{\partial\xi\partial\psi}\sec\theta\right)^2\Bigg]\cos\theta d\xi d\psi. \end{aligned} \quad (12)$$

Rayleigh-Ritz method requires that maximum strain energy must be equal to maximum kinetic energy i.e.,:

$$J = \delta(V_s - T_s) = 0. \quad (13)$$

From Eqs. (1), (6-9), we have:

$$
\begin{aligned}
J = \int_0^a \int_0^b \Bigg[& \left\{\left\{1-\alpha\left(1-\frac{\xi}{a}\right)\left(1-\frac{\psi}{b}\right)\right\}\{(1+\beta\Upsilon_1)\}^3\right\}\left\{\cos^4\theta+\frac{E_2}{E_1}\sin^4\theta\right. \\
& \left.+2\nu_\psi\sin^2\theta\cos^2\theta\right\}\left(\frac{\partial^2\Phi}{\partial\xi^2}\right)^2+\left\{4\frac{G_0}{E_1}\left(1-\nu_{\xi_0}(1-m\Upsilon_1)\nu_\psi\right)\sin^2\theta\cos^2\theta\right\}\left(\frac{\partial^2\Phi}{\partial\xi^2}\right)^2 \\
& +\frac{E_2}{E_1}\left(\frac{\partial^2\Phi}{\partial\psi^2}\right)^2+4\left\{\frac{E_2}{E_1}\sin^2\theta+\frac{G_0}{E_1}\left(1-\nu_{\xi_0}(1-m\Upsilon_1)\nu_\psi\right)\cos^2\theta\right\}\left(\frac{\partial^2\Phi}{\partial\xi\partial\psi}\right)^2 \\
& +2\left\{\frac{E_2}{E_1}\sin^2\theta+\nu_\psi\cos^2\theta\right\}\left(\frac{\partial^2\Phi}{\partial\xi^2}\right)\left(\frac{\partial^2\Phi}{\partial\psi^2}\right) \\
& -4\left\{\frac{E_2}{E_1}\sin^3\theta+2\nu_\psi\sin\theta\cos^2\theta\right\}\left(\frac{\partial^2\Phi}{\partial\xi^2}\right)\left(\frac{\partial^2\Phi}{\partial\xi\partial\psi}\right) \\
& +2\left\{\frac{G_0}{E_1}\left(1-\nu_{\xi_0}(1-m\Upsilon_1)\nu_\psi\right)\sin\theta\cos^2\theta\right\}\left(\frac{\partial^2\Phi}{\partial\xi^2}\right)\left(\frac{\partial^2\Phi}{\partial\xi\partial\psi}\right) \\
& -4\left\{\frac{E_2}{E_1}\sin\theta\right\}\left(\frac{\partial^2\Phi}{\partial\psi^2}\right)\left(\frac{\partial^2\Phi}{\partial\xi\partial\psi}\right)\Bigg]d\xi d\psi-\lambda^2\int_0^a\int_0^b[(1-m\Upsilon_1)(1+\beta\Upsilon_1)]\Phi^2 d\xi d\psi,
\end{aligned}
\tag{14}
$$

where $\lambda^2=\frac{12\rho_0 a^2\cos^5\theta}{E_1^* h_0^2}$, $\Upsilon_1=\left(1-\sqrt{1-\frac{\xi^2}{a^2}}\right)$.

The two term deflection function which satisfy all the edge conditions can be taken as in [7]
The two term deflection function which satisfy all the edge conditions can be taken as in [7]:

$$
\Phi(\xi,\psi)=\left[\left(\frac{\xi}{a}\right)^e\left(\frac{\psi}{b}\right)^f\left(1-\frac{\xi}{a}\right)^g\left(1-\frac{\psi}{b}\right)^h\right]\times\left[\sum_{i=0}^{N}\Omega_i\left\{\left(\frac{\xi}{a}\right)\left(\frac{\psi}{b}\right)\left(1-\frac{\xi}{a}\right)\left(1-\frac{\psi}{b}\right)\right\}^i\right]. \tag{15}
$$

This expression results from two components: one defining boundary conditions (0 for free edge, 1 for simply supported, 2 for clamped edge), and the other representing mode frequencies with constants Ω_i for $i=0,1,2,\cdots,N$. To minimize the functional in Eq. (11), the following condition is necessary:

$$
\frac{\partial J}{\partial\Omega_i}=0,\quad i=0,1,2,3\ldots N. \tag{16}
$$

After simplifying Eq. (13), we get a homogeneous system of equations in Ω_i whose non zero solution gives equation of frequency as:

$$
|P-\lambda^2 Q|=0, \tag{17}
$$

where, $P=\left[p_{ij}\right]_{N+1}$ and $Q=[qij]_{N+1}$ are square matrices of order $(n+1)$ with $i=0,1,2\ldots N$ and $j=0,1,2\ldots N$. The time period is calculated using the expression:

$$
K=\frac{2\pi}{\lambda}, \tag{18}
$$

where λ is a frequency obtained from Eq. (14).

3. Numerical results and discussion

This study investigated the impact of parameters such as tapering, thermal gradient, and non-homogeneity on the vibration time period of an orthotropic parallelogram plate. The plate had a fixed aspect ratio of $a/b = 1.5$, a skew angle of $\theta = 30°$, circular thickness, and Poisson's ratio. The analysis considered specific edge conditions and linear temperature effects, with material parameters sourced from [5]: $E_2^*/E_1^* = 0.01$, $E^*/E_1^* = 0.3$, $G_0/E_1^* = 0.0333$, $E_1^*/\rho_0 = 3.0\times10^5$ and $\nu_{\xi_0} = 0.345$. The results are presented in Tables 1-3.

Table 1. Time period of orthotropic parallelogram plate at $SCCC$ edge condition corresponding to non-homogeneity parameter m

	m	α = 0.2									
		β = 0.0		β = 0.2		β = 0.4		β = 0.6		β = 0.8	
		K_2	K_1	K_2	K_1	K_2	K_1	K_2	K_1	K_2	K_1
SCCC	0.0	0.44915	0.07578	0.44001	0.07564	0.43034	0.07543	0.42022	0.07515	0.40973	0.07480
	0.2	0.44909	0.07577	0.43995	0.07563	0.43027	0.07542	0.42013	0.07515	0.40963	0.07479
	0.4	0.44903	0.07577	0.43989	0.07563	0.43021	0.07542	0.42006	0.07514	0.40954	0.07479
	0.6	0.44897	0.07577	0.43982	0.07563	0.43015	0.07542	0.42000	0.07514	0.40948	0.07479
	0.8	0.44893	0.07577	0.43976	0.07563	0.43005	0.07542	0.41991	0.07514	0.40938	0.07478

Table 2. Time period of orthotropic parallelogram plate at $SCCC$ edge condition corresponding to thermal gradient α

	α	m = 0.2									
		β = 0.0		β = 0.2		β = 0.4		β = 0.6		β = 0.8	
		K_2	K_1	K_2	K_1	K_2	K_1	K_2	K_1	K_2	K_1
SCCC	0.0	0.43238	0.07212	0.42396	0.07202	0.41501	0.07186	0.40564	0.07163	0.39594	0.07134
	0.2	0.44909	0.07577	0.43995	0.07563	0.43027	0.07542	0.42013	0.07515	0.40963	0.07479
	0.4	0.46807	0.08004	0.45808	0.07985	0.44752	0.07958	0.43643	0.07923	0.42500	0.07880
	0.6	0.48996	0.08512	0.47894	0.08485	0.46725	0.08450	0.45503	0.08406	0.44240	0.08352
	0.8	0.51573	0.09130	0.50335	0.09093	0.49022	0.09046	0.47655	0.08989	0.46247	0.08921

Table 3. Time period of orthotropic parallelogram plate at $SCCC$ edge condition corresponding to tapering parameter β

	β	$m = \alpha = 0.0$		$m = \alpha = 0.2$		$m = \alpha = 0.4$		$m = \alpha = 0.6$		$m = \alpha = 0.8$	
		K_2	K_1	K_2	K_1	K_2	K_1	K_2	K_1	K_2	K_1
SCCC	0.0	0.43244	0.07213	0.44909	0.07577	0.46800	0.08004	0.48984	0.08511	0.51551	0.09129
	0.2	0.42402	0.07202	0.43995	0.07563	0.45801	0.07985	0.47878	0.08485	0.50310	0.09092
	0.4	0.41510	0.07186	0.43027	0.07542	0.44743	0.07958	0.46706	0.08450	0.48996	0.09045
	0.6	0.40574	0.07163	0.42013	0.07515	0.43637	0.07923	0.45484	0.08405	0.47627	0.08988
	0.8	0.39600	0.07134	0.40963	0.07479	0.42490	0.07880	0.44221	0.08352	0.46216	0.08920

Table 1 presents time period data for an orthotropic parallelogram plate under the $SCCC$ edge condition and a constant thermal gradient ($\alpha = 0.2$). The table covers a range of non-homogeneity parameter (m) and tapering parameter (β) values from 0.0 to 0.8. The results show that higher β values lead to a decrease in time period K, similar to the effect of increasing m on reducing K.

Table 2 exhibits time period (K) data for an orthotropic parallelogram plate under the $SCCC$ edge condition, with a constant non-homogeneity parameter ($m = 0.2$). The table encompasses β and α values from 0.0 to 0.8. Remarkably, higher thermal gradient (α) values result in elevated time period (K), while increasing the tapering parameter (β) leads to a significant decrease in K.

Table 3 presents time periods for an orthotropic parallelogram plate under the $SCCC$ edge condition, with variable non-homogeneity (m), thermal gradient (α), and tapering (β) parameters ranging from 0.0 to 0.8. Higher values of α and m lead to an increase in the time period (K), while raising β results in a reduction of K.

4. Conclusions

In terms of time periods, Table 1 indicates that β holds greater influence than m under the $SCCC$ edge condition. Additionally, in Tables 2 and 3, β demonstrates a more substantial effect on the time period's rate of change compared to α and m, respectively.

Acknowledgements

The authors have not disclosed any funding.

Data availability

The datasets generated during and/or analyzed during the current study are available from the corresponding author on reasonable request.

Conflict of interest

The authors declare that they have no conflict of interest.

References

[1] A.W. Leissa, "Vibration of plates scientific and technical information division," National Aeronautics and Space Administration, 1969.

[2] M. Di Sciuva, "Bending, vibration and buckling of simply supported thick multilayered orthotropic plates: An evaluation of a new displacement model," *Journal of Sound and Vibration*, Vol. 105, No. 3, pp. 425–442, Mar. 1986, https://doi.org/10.1016/0022-460x(86)90169-0

[3] A. K. Gupta and Mamta, "Effect of exponential temperature variation on frequencies of a rectangular plate of non-linear varying thickness," *American Journal of Applied Sciences*, Vol. 10, No. 2, 2019.

[4] A. K. Gupta, A. Kumar, and H. Kaur, "Vibration of visco-elastic orthotropic parallelogram plate with linear thickness variation in both directions," *International Journal of Acoustics and Vibration*, Vol. 2, pp. 72–80, 2011.

[5] A. K. Gupta, A. Kumar, and D. V. Gupta, "Vibration of visco-elastic orthotropic parallelogram plate with parabolically thickness variation," *Annals of the Faculty of Engineering Hunedoara*, Vol. 10, No. 2, pp. 61–70, 2012.

[6] A. Khanna and A. Singhal, "Effect of plate's parameters on vibration of isotropic tapered rectangular plate with different boundary conditions," *Journal of Low Frequency Noise, Vibration and Active Control*, Vol. 35, No. 2, pp. 139–151, 2016.

[7] N. Lather, R. Bhardwaj, A. Sharma, K. Kumar, and A. L. Schiavo, "Time period analysis of orthotropic skew plate with 2-D circular thickness and 1-D circular density," *Mathematical Problems in Engineering*, Vol. 2022, pp. 1–15, 2022.

[8] A. Sharma, "Natural vibration of parallelogram plate with circular variation in density," *Acta Technica*, Vol. 63, No. 6, pp. 763–774, 2018.

[9] A. Sharma, A. Raghav, and V. Kumar, "Mathematical study of vibration on non-homogeneous parallelogram plate with thermal gradient," *International Journal of Mathematical Sciences*, Vol. 9, No. 2, 2016.

[10] A. K. Sharma and M. K. Dhiman, "Vibration analysis of simply supported parallelogram plate with bi-dimensional thickness and temperature deviation," *International Journal of Research in Advent Technology*, Vol. 6, No. 12, 2018.

[11] A. K. Sharma and V. Verma, "Inspection of vibration using Rayleigh-Ritz method for orthotropic non-homogeneous plate with varying thickness and thermal effect," *Romanian Journal of Acoustics and Vibration*, Vol. 14, No. 1, 2017.

[12] A. K. Sharma, M. K. Dhiman, H. Singh, P. Prashar, and P. Sharma, "Effect of non-homogeneity with thickness and temperature variation on vibration of orthotropic parallelogram plate with simply supported edges.," *ARPN Journal of Engineering and Applied Sciences*, Vol. 14, No. 15, pp. 2757–2762, 2006.